Advances in Forest Fire Research

2018

EDITED BY

DOMINGOS XAVIER VIEGAS

ADAI/CEIF, UNIVERSITY OF COIMBRA, PORTUGAL

A study of the structure of a turbulent line fire subjected to cross-flow using large eddy simulations

Arnaud Trouvé*; Salman Verma

Department of Fire Protection Engineering, University of Maryland. College Park, MD, 20742, USA, {atrouve@umd.edu, salman.iaal@gmail.com}*

Abstract

The general objective of this project is to provide a basic understanding of the transition between the different flame regimes observed in fires with cross-flow and/or fires along inclined surfaces. We consider here a simplified configuration corresponding to a methane-air, buoyancy-driven, turbulent line flame stabilized on top of a horizontal floor surface and subjected to different air cross-flow velocities. At high values of the cross-flow velocity, the flame features a horizontal shape and develops as a boundary layer flame in the vicinity of the floor surface; the flow downstream of the flame is attached to the floor surface and air entrainment into the flame is one-sided. In contrast, at low values of the cross-flow velocity, the flame features a tilted vertical shape and develops as a pool-like flame; the flow downstream of the flame separates from the floor surface and air entrainment into the flame is two-sided. In the present study, we analyze the transition from an attached flame to a lifted flame using wall-resolved large eddy simulations (LES). Simulations are performed with an LES solver developed by FM Global and called FireFOAM. The simulated line burner is 50-cm wide and 5-cm long; the flame power is 50 kW; and the air cross-flow velocities range between 0.75 and 3 m/s. The LES simulations provide a detailed description of the different contributions to flow kinetic energy in the horizontal and vertical directions and thereby provide unique insights into the competing effects of the external momentum of the horizontal cross-flow and the internal momentum of the vertical buoyant motions produced by the combustion heat release and the resulting unstable thermal stratification. A new criterion is proposed to measure the relative strength of external/cross-flow-driven versus internal/buoyancy-driven motions and to thereby predict the transition from an attached to a lifted flame regime.

Keywords: Buoyant turbulent diffusion flame; Wind-driven flames; Boundary layer flame; Pool flame; Air entrainment; Large Eddy Simulation

1. Introduction

Developing a fundamental understanding of the effects of cross-flow on fires is of considerable interest in fire science; because of the ubiquity and importance of such effects in wildland, urban and industrial fires. One basic way in which cross-flow affects a fire is by changing the flame geometry: as the external momentum of the horizontal cross-flow increases, the flame transitions from a vertical pool-like flame to a horizontal flame attached to the downstream surface (Tang *et al.* 2017). Among other things, attachment of the flame increases the convective heat transfer to the downstream surface; this in turn increases the rate of flame spread (in cases for which the downstream surface contains fresh fuel).

The variations in flame geometry in fires subjected to cross-flow have been studied both experimentally (Putnam 1965; Oka *et al.* 2000; Oka *et al.* 2003; Cole *et al.* 2011; Hu *et al.* 2013; Lam and Weckman 2015) and numerically (Albini 1981; Sinai and Owens 1995; Morvan *et al.* 1998; Porterie *et al.* 2000; Morvan *et al.* 2001; Nmira *et al.* 2010; Vasanth *et al.* 2013) over the past several decades. However, past experimental studies typically use a limited range of diagnostics, primarily video imaging and temperature measurements, while past numerical studies typically use low-order approaches, for instance Reynolds-Averaged Navier-Stokes simulations (Sinai and Owens 1995;

Morvan *et al.* 1998; Porterie *et al.* 2000; Morvan *et al.* 2001; Nmira *et al.* 2010; Vasanth *et al.* 2013), that do not resolve the relevant turbulent flow and flame scales. Thus, a basic understanding of the physics associated with variations in wind-driven flame geometry is lacking and is the primary motivation behind the present study.

In the present study, a methane-fueled, buoyancy-driven, turbulent line flame stabilized on top of a horizontal floor surface and subjected to different cross-flow velocities is simulated using wall-resolved Large Eddy Simulations (LES). The primary objective is to gain fundamental insights into the transition from a vertical to a horizontal flame resulting from increases in the cross-flow velocity. In what is seen as an intermediate step, the present study considers a gas-fueled turbulent flame that is non-spreading, is statistically stationary and that therefore lends itself to simplified analysis. Configurations that are closer to wildland fire configurations and that feature representative vegetation fuel and spreading flames will be considered in future work.

2. Numerical Solver and Configuration

Numerical simulations are performed using FireFOAM (FireFOAM 2018), a fire modeling solver developed by FM Global and based on an open-source, general-purpose, Computational Fluid Dynamics (CFD) software package called OpenFOAM (OpenFOAM 2018). FireFOAM is a second-order accurate, finite volume solver with implicit time integration; the solver features advanced meshing capabilities (structured/unstructured polyhedral mesh); it also features a massively parallel computing capability using Message Passing Interface protocols.

FireFOAM uses a Favre-filtered, compressible-flow, LES formulation and provides a choice between several modeling options for the treatment of turbulence, combustion and thermal radiation. In the present study: subgrid-scale (SGS) turbulence is described using the WALE (Wall-Adapting Local Eddy-viscosity) model (Nicoud and Ducros 1999); combustion is described using the classical concept of a global combustion equation combined with the Eddy Dissipation Concept (EDC) model (Magnussen and Hjertager 1977); radiation is described by solving the radiative transfer equation (RTE) using a discrete-ordinates, finite-volume method and by assuming a non-scattering, non-absorbing, optically-thin medium and using a prescribed global radiative loss fraction χ_{rad}.

The numerical configuration is presented in Fig. 1. The computational domain is 780-cm-long in the streamwise x-direction, 50-cm-wide in the spanwise y-direction and 250-cm-high in the vertical z-direction. The line burner face is 5-cm-long in the x-direction and 50-cm-wide in the y-direction; and the spanwise center of its leading edge is placed at the origin $(x,y,z) = (0,0,0)$. The burner is flush-mounted on a 50-cm-wide horizontal solid plate that starts at $x = (-20)$ cm and ends at $x = 205$ cm. The cross-flow air is injected through a 50-cm-wide and 50-cm-high wind tunnel whose outlet is located at the inlet boundary of the computational domain, at $x = (-30)$ cm. A 5-mm-long, 50-cm-wide and 5-mm-high trip wire is placed at $x = (-10.5)$ cm in order to perturb the incoming flow and promote laminar-to-turbulent transition.
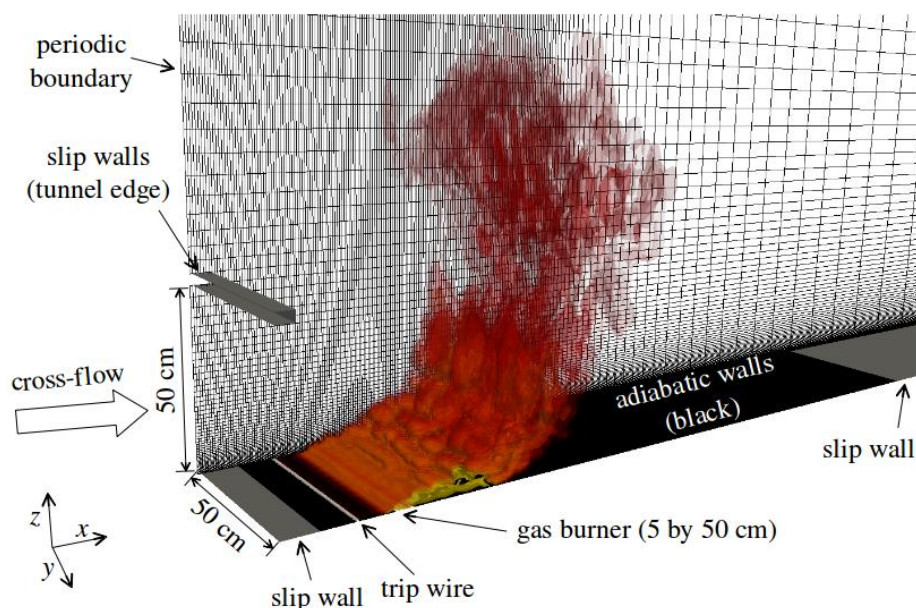
Figure 1 - Illustration of the FireFOAM numerical configuration; the 50 kW methane diffusion flame is visualized using isocontours of instantaneous volumetric heat release rate (0.1, 1, 10, 100, 1000, 10000 kW/m3).

The computational grid is a rectangular Cartesian mesh. Grid spacing in the streamwise x-direction is uniform and is equal to 5 mm for $x \leq 100$ cm; beyond that location, the x-grid is stretched with a stretch factor equal to 1.06. Grid spacing in the spanwise y-direction is uniform and is equal to 5 mm. This streamwise (spanwise) resolution corresponds to 10 (100) grid cells across the burner length (width). Grid spacing in the vertical z-direction is non-uniform: the z-grid spacing is 1.2 mm at $z = 0$ (*i.e*, the first cell center is 0.6 mm above the south boundary of the computational domain) and is 20 mm at $z = 50$ cm with a stretching factor of 1.04. For $z \geq 50$ cm, the z-grid is stretched with a stretch factor equal to 1.06. Note that with the present resolution, the trip wire is under-resolved and is described with 1 (4) grid cell(s) in the x- (z-) direction. The total number of cells is 3.5 million.

The methane mass flow rate is prescribed at the burner boundary and the air velocity is fixed at the tunnel outlet. The horizontal solid plate and the trip wire are both treated as no-slip adiabatic solid walls. The surface located at $z = 0$ between the tunnel outlet and the leading edge of the solid plate is treated as a slip wall. The surface located at $z = 0$ beyond the solid plate, at $x \geq 205$ cm, is also treated as a slip wall. The side boundaries at $y = (-25)$ and 25 cm correspond to periodic conditions. Other boundaries are treated as boundaries with open flow conditions.

In all cases, the methane mass flow rate is linearly increased from 0 to 1 g/s during the first five seconds and is then held constant for the remainder of the simulations. This is done to allow the cross-flow to establish itself over the line burner before the fire reaches its nominal value of the heat release rate equal to 50 kW. All simulations are performed for a duration of 30 s. Turbulent statistics are collected for the final 15 s of each simulation, after the flow and flame become statistically stationary and long enough for the statistics to be converged (to improve convergence, statistics are computed using both temporal- and spanwise-averaging). The time step is controlled by a classical Courant-Friedrichs-Lewy (CFL) condition and is approximately equal to 0.35 ms. Each simulation is run using 200 processors on a large-scale Linux cluster with a typical simulation requiring 40,000 CPU-hours.

3. Results and Discussion

We first consider the mean flame shape for a range of cross-flow velocities (Fig. 2). As U_∞ increases from 0.75 to 3 m/s, the flame transitions from a lifted (vertically tilted) flame to an attached (horizontal)

flame. The vertical elevation of the flame decreases (from 50 to 10 cm); the flame length (loosely defined as the distance from the burner to the flame tip) increases (from 50 to 100 cm); and the flame attachment length (defined as the *x*-wall-distance downstream of the burner within the flame region) increases (from 30 to 90 cm). In the present configuration the transition from a vertical tilted flame to a horizontal flame is gradual and happens between $U_\infty = 1$ and 1.5 m/s.
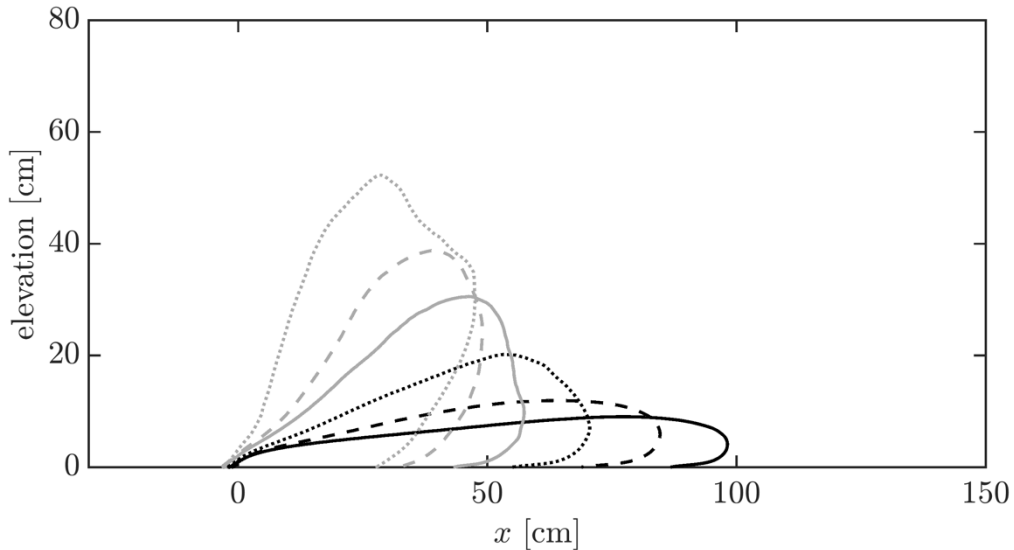

Figure 2 - Mean flame shape visualized using a particular isoline of the mean heat release rate per unit volume (50 kW/m³). From left to right: U_∞ = 0.75, 1, 1.25, 1.5, 2, 3 m/s.

We then consider the mean plume shape for the six different cases (Fig. 3). The plume, in contrast to the flame, transitions much more abruptly; for instance, the plume shape changes drastically (from vertically tilted to horizontal) when U_∞ is increased from 1.5 to 2 m/s.
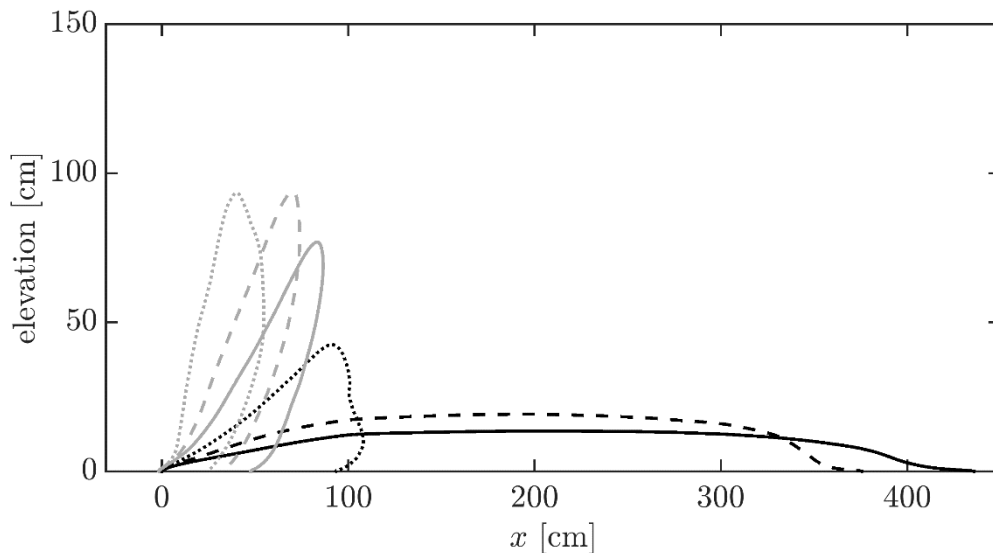

Figure 3 - Mean plume shape visualized using a particular isoline of the mean temperature (400 K). From left to right: U_∞ = 0.75, 1, 1.25, 1.5, 2, 3 m/s.

We now consider the spatial variations of mean velocity vector ($\overline{U}, \overline{W}$) for two cases, $U_\infty = 0.75$ and 3 m/s (Fig. 4). In the 0.75-m/s case, the cross-flow is strongly deflected upwards; in addition, a reversed flow is induced by the flame on the downwind side leading to two-sided entrainment similar to pool

fires. In contrast, in the 3-m/s case, the cross-flow is only weakly affected by the presence of the flame and entrainment is one-sided due to the flame being attached to the downstream surface. These differences in flow pattern are known to be key ingredients in flame spread mechanisms (Dold and Zinoviev 2009).
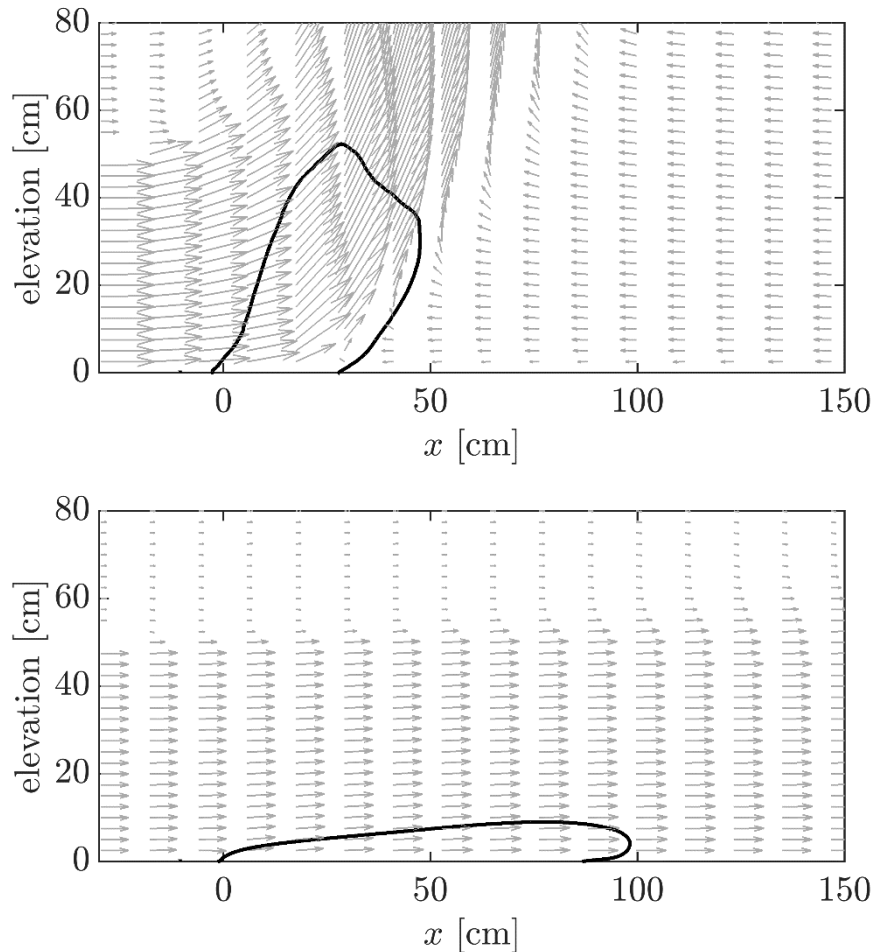

Figure 4 - Spatial variations of the mean flow velocity vector ($\overline{U}$, $\overline{W}$): $U∞$=0.75 m/s (top); $U∞$=3 m/s (bottom). Solid lines are isolines of the mean heat release rate per unit volume (50 kW/m3) and are used for marking the flame region.

Figure 5 presents *z*-profiles of different quantities of interest ($\overline{U}$, $\overline{W}$, U_{rms}, W_{rms}, B_z and S_{xz}) across the flame zone, at $x = 50$ cm and for $U_∞ = 1.5$ m/s. U_{rms} (W_{rms}) is defined as the mean amplitude of temporal fluctuations of the grid-resolved streamwise (vertical) flow velocity component; and B_z and S_{xz} are the source terms responsible for producing turbulent kinetic energy in the *z*- and *x*-directions, respectively, $B_z=(\overline{-w''(\partial \overline{p}/\partial z)})$ and $S_{xz}=(\overline{-\rho u''w''(\partial \tilde{u}/\partial z)})$, where $\overline{q}$ ($\tilde{q}$) designates a straight (mass-weighted) temporal mean of a grid-resolved quantity q, and $q''= (q-\tilde{q})$. B_z represents production of (vertical) turbulence by buoyancy whereas S_{xz} represents production of (horizontal) turbulence by shear.

The case with $U_∞$=1.5-m/s is important because this flame is close to the point of transition between the horizontal and vertical flame regimes. Figure 5 shows that: turbulence production in the flame zone is dominated by buoyancy (B_z is much larger than S_{xz}); the flow activity in the vertical direction is strongly turbulent ($W_{rms} > \overline{W}$); and the vertical turbulent velocities take values that have the same order of magnitude as those of the cross-flow velocity ($W_{rms} = O(U_∞)$). These results suggest that flow deflection and the establishment of a vertically-oriented flame is a consequence of the vertical turbulent motions produced by buoyancy.
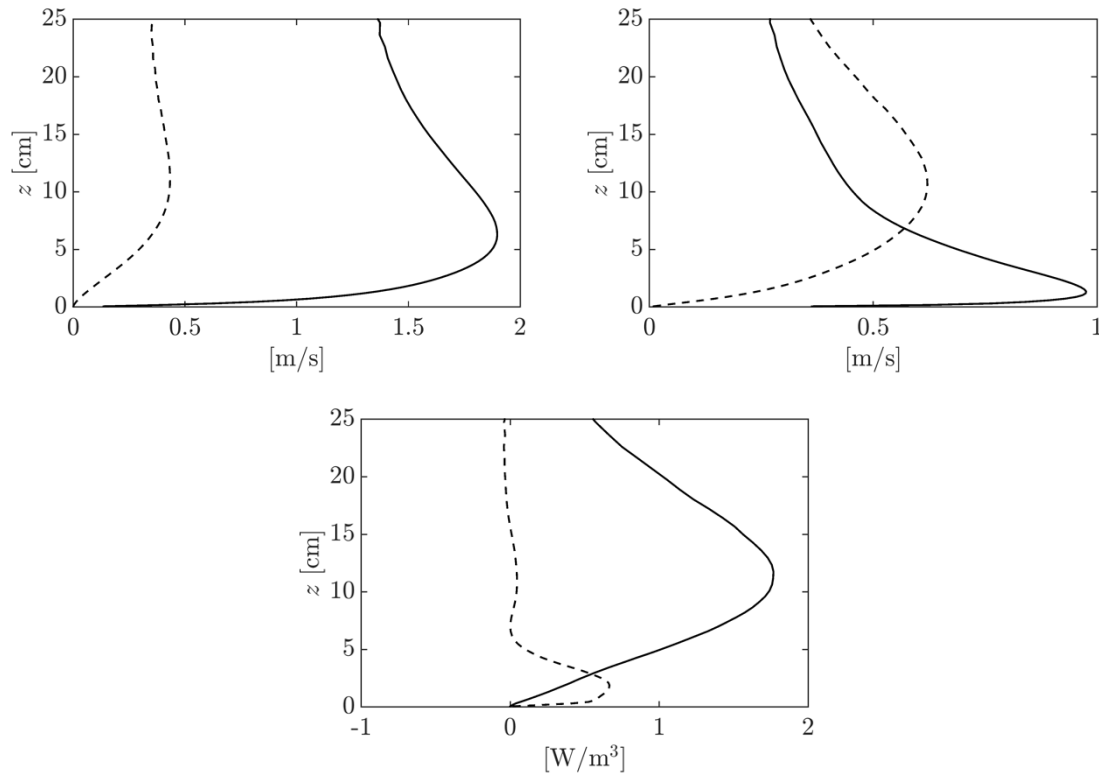
Figure 5 - Vertical profiles for U_∞ = 1.5 m/s at x = 50 cm: $\overline{U}$ and $\overline{W}$ (top left); U_{rms} and W_{rms} (top right); B_z and S_{xz} (bottom). $\overline{U}$, U_{rms}, B_z ($\overline{W}$, W_{rms}, S_{xz}) are plotted using solid (dashed) lines.

The magnitude of this effect can be measured globally by spatially-integrating the source term B_z and by comparing the resulting integrated value to the flow rate of kinetic energy (or equivalently the power) of the incoming cross-flow. We write:

$$R = \frac{\left(\int_0^{L_x}\left(\int_0^{L_z} B_z dz\right)dx\right) L_y}{\frac{1}{2}\rho_\infty U_\infty^3 L_z L_y} = \frac{\left(\int_0^{L_x}\left(\int_0^{L_z} B_z dz\right)dx\right)}{\frac{1}{2}\rho_\infty U_\infty^3 L_z} \qquad (1)$$

where R is the ratio of the power of the production of z-turbulence due to buoyancy divided by the power of the incoming cross-flow. In Eq. 1, ρ_∞ is the air mass density, and L_x, L_y and L_z are the x-, y- and z-sizes of the control volume under consideration (due to periodicity in the y-direction, L_y is simply dropped).

Figure 6 presents the variations of the power ratio R with streamwise distance using $L_x = x$ and $L_z = H_t$ ($H_t = 50$ cm is the wind tunnel height). With these choices for L_x and L_z, R represents the cumulative effects of production of vertical turbulence by buoyancy up to a given location x compared to the total power of the flow delivered by the wind tunnel. We expect significant flow deflection and a transition from an upwind horizontal flame to a downwind vertical flame when R takes values close to or above 1 prior to the end of the flame zone. Figure 6 shows that the 1.25-m/s-flame reaches a peak value of R equal to 0.4 and that the 1-m/s-flame reaches a peak value above 1. These estimates suggest that the 1.25-m/s-flame is in the transitional regime while the 1-m/s flame is in the vertical flame regime.
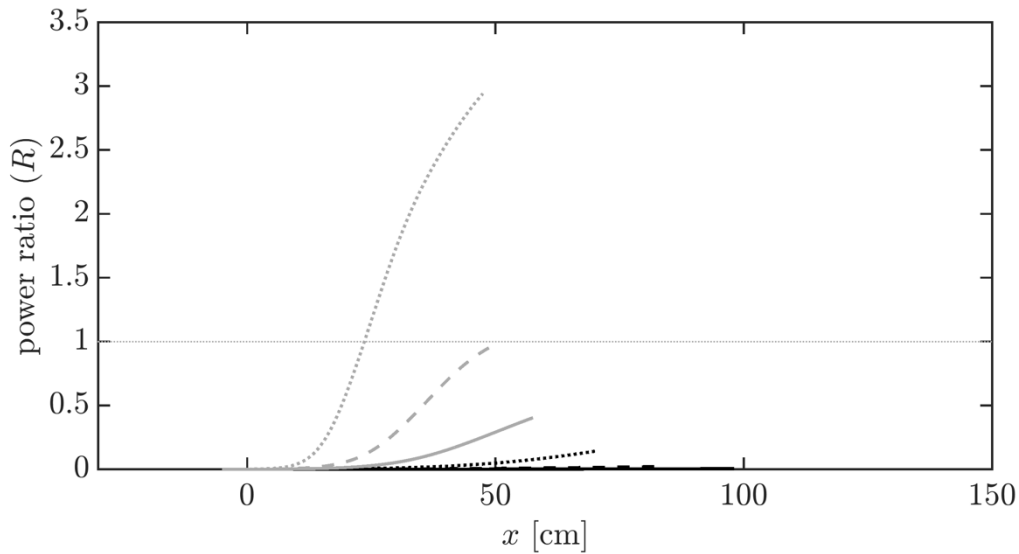
Figure 6 - Streamwise evolution of the power ratio R (see Eq. 1), plotted from x = 0 to the downstream x-location of the flame tip. From left to right: U∞ = 0.75, 1, 1.25, 1.5, 2, 3 m/s; note that the 2- and 3-m/s curves correspond to low values of R and are horizontal.

It is worth noting that the power ratio R introduced in the present study is similar to, but different from Byram's convection number N_C, defined as:

$$N_C = \frac{gI}{\frac{1}{2}\rho_\infty U_\infty^3 c_p T_\infty} \qquad (2)$$

where g is the acceleration of gravity, I the fireline intensity (in the present configuration $I = 100$ kW/m), c_p the specific heat of ambient air at constant pressure and T_∞ the ambient temperature. Like R, N_C is a power ratio that compares the effect of buoyancy to that of the cross-flow (Nelson 1993); compared to R, N_C has the advantage to explicitly bring out the effect of the fire power through I (in the expression of R, this effect is implicit through B_z); but unlike R, N_C does not account for x-variations and therefore cannot predict the streamwise location where a possible change in flame or plume structure may occur.

Using standard scaling arguments as well as some guidance from the simplified flame/plume models proposed by Albini (1981) and Nelson *et al.* (2012), a possible expression for R is as follows:

$$R = C_R N_C^{\frac{1}{2}} \left(\frac{g(\Delta T_{flame}/T_\infty)x}{U_\infty^2} \right) \qquad (3)$$

where ΔT_{flame} denotes the mean excess flame temperature and C_R is a model coefficient. In the following, we use $\Delta T_{flame} = 305$ K and $C_R = 0.057$.

Figure 7 presents a comparison of the model expression for R given in Eq. (3) with its definition given in Eq. (1), as obtained from the LES simulations. It is found that the model expression for R has some limitations: it varies linearly with x and is not able to represent the higher order streamwise variations observed in the LES data. It is also found, however, that the expression in Eq. (3) is capable of capturing the changes in the values of the power ratio associated with changes in the cross-flow velocity. Work is currently in progress in order to determine whether the model expression for R can be used to predict the streamwise location where a change in flame or plume structure will occur.
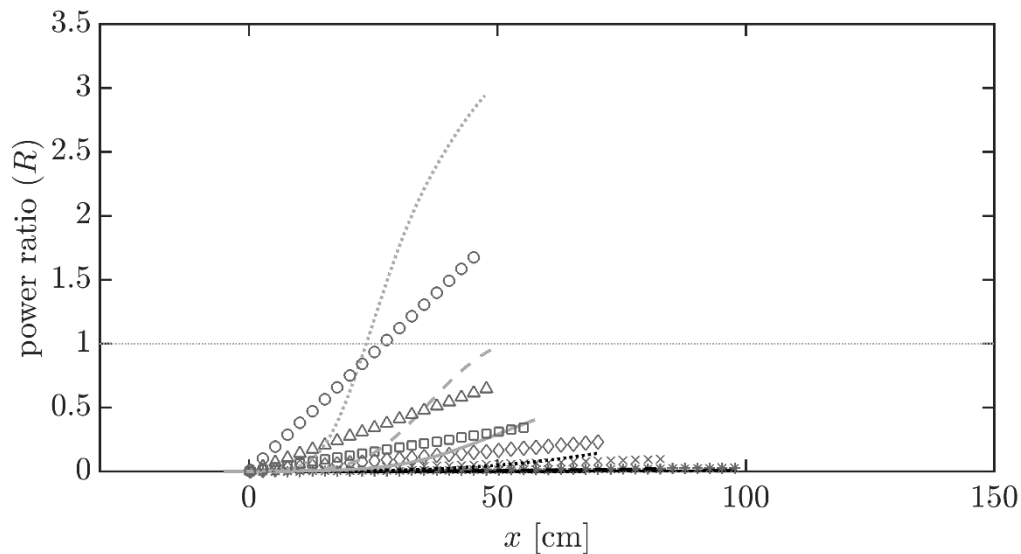
Figure 7 - Streamwise evolution of the power ratio R, plotted from x = 0 to the downstream x-location of the flame tip. From left to right: U∞ = 0.75, 1, 1.25, 1.5, 2, 3 m/s. Comparison between Eq. (1) (solid lines) and Eq. (3) (symbols).

4. Conclusions

Fine-grained LES are performed to bring fundamental insight into the effects of cross-flow velocity on the structure of a methane-air, buoyancy-driven, turbulent line flame (50 kW) stabilized on top of a horizontal floor surface. As the cross-flow velocity is increased, the flame transitions from a pool-like flame characterized by a tilted vertical shape to a boundary layer flame characterized by a horizontal shape. The pool-like flame strongly deflects the incoming cross-flow upwards and features downwind flow separation and two-sided air entrainment into the flame. In contrast, the boundary layer flame does not significantly deflect the incoming cross-flow and features downwind flow attachment and one-sided air entrainment into the flame.

The present simulations are analyzed in terms of production of mean flow and turbulent flow kinetic energy. Results suggest that the transition between the (vertical) pool-like and (horizontal) boundary layer flame regimes is controlled by the strength of the vertical turbulent motions produced by buoyancy. A new non-dimensional number that measures the ratio of the power of the production of z-turbulence due to buoyancy divided by the power of the incoming cross-flow is introduced to explain the transition.

5. Acknowledgments

6. References

Albini FA (1981) A model for the wind-blown flame from a line fire. *Combustion and Flame* 43, 155-174.

Cole WJ, Dennis MH, Fletcher TH, Weise DR (2011) The effects of wind on the flame characteristics of individual leaves. *International Journal of Wildland Fire* 20, 657-667.

Dold JW, Zinoviev A (2009) Fire eruption through intensity and spread rate interaction mediated by flow attachment. *Combustion Theory and Modelling* 13, 763-793.

FireFOAM (2018) Developed by FM Global, available at: https://github.com/fireFoam-dev.

Hu L, Wu L, Liu S (2013) Flame length elongation behavior of medium hydrocarbon pool fires in cross air flow. *Fuel* 111, 613-620.

Lam CS, Weckman EJ (2015) Wind-blown pool fire, Part I: Experimental characterization of the thermal field. *Fire Safety Journal* 75, 1-13.

Magnussen BF, Hjertager BH (1977). On mathematical modeling of turbulent combustion with special emphasis on soot formation and combustion. *Symposium (international) on Combustion* 16, 719-729.

Morvan D, Porterie B, Larini M, Loraud JC (1998) Numerical simulation of turbulent diffusion flame in cross flow. *Combustion Science and Technology* 140, 93-122.

Morvan D, Porterie B, Loraud JC, Larini M (2001) A numerical investigation of cross wind effects on a turbulent buoyant diffusion flame. *Combustion Science and Technology* 164, 1-35.

Nelson RM (1993) Byram's derivation of the energy criterion for forest and wildland fires. *International Journal of Wildland Fire* 3, 131-138.

Nelson RM, Butler BW, Weise DR (2012) Entrainment regimes and flame characteristics of wildland fires. *International Journal of Wildland Fire* 21, 127–140.

Nicoud F, Ducros F (1999) Subgrid-scale stress modelling based on the square of the velocity gradient tensor. *Flow, Turbulence and Combustion* 62, 183-200.

Nmira F, Consalvi JL, Boulet P, Porterie B (2010) Numerical study of wind effects on the characteristics of flames from non-propagating vegetation fires. *Fire Safety Journal*, 45, 129-141.

Oka Y, Kurioka H, Satoh H, Sugawa O (2000) Modelling of unconfined flame tilt in cross-winds. *Fire Safety Science* 6, 1101-1112.

Oka Y, Sugawa O, Imamura T, Matsubara Y (2003) Effect of cross-winds to apparent flame height and tilt angle from several kinds of fire source. *Fire Safety Science* 7, 915-926.

OpenFOAM (2018) Developed by the OpenFOAM foundation, available at: http://www.openfoam.org.

Porterie B, Morvan D, Loraud JC, Larini M (2000) Firespread through fuel beds: modeling of wind-aided fires and induced hydrodynamics *Physics of Fluids* 12, 1762-1782.

Putnam AA (1965) A model study of wind-blown free-burning fires. *Symposium (International) on Combustion* 10, 1039-1046.

Sinai YL, Owens MP (1995) Validation of CFD modelling of unconfined pool fires with cross-wind: flame geometry. *Fire Safety Journal* 24, 1-34.

Tang W, Miller CH, Gollner MJ (2017) Local flame attachment and heat fluxes in wind-driven line fires. *Proceedings of the Combustion Institute* 36, 3253-3261.

Vasanth S, Tauseef SM, Abbasi T, Abbasi SA (2013) Assessment of four turbulence models in simulation of large-scale pool fires in the presence of wind using computational fluid dynamics (CFD). *Journal of Loss Prevention in the Process Industries* 26, 1071-1084.